Influence of Crystal Effects on Molecular Charge Densities in a Study of 9-Ethynyl-9-fluorenol

Jacob Overgaard,[†] Mark P. Waller,[†] James A. Platts,[‡] and David E. Hibbs*[,†]

School of Chemistry, Building F11, University of Sydney, NSW 2006, Sydney, Australia, and Chemistry Department, P.O. Box 912, Cardiff University, Cardiff CF10 3TB, U.K.

Received: August 3, 2003; In Final Form: September 30, 2003

The experimental charge density distribution in crystalline 9-ethynyl-9-fluorenol has been determined in a refinement of a pseudo-atomic multipolar expansion (Hansen−Coppens formalism) against extensive low-temperature (T = 100 K) single-crystal X-ray diffraction data and compared with a selection of theoretical DFT calculations on the same complex. The molecule crystallizes in the centrosymmetric space group $C2/c$ with two independent molecules in the asymmetric unit. A range of multipole models of varying complexity were tested and found to describe the observed intensities almost equally well in terms of the usual residual values presented; however, the resulting total density distributions and derived properties, such as atomic charges and molecular electrostatic potentials, showed significant differences and it is emphasized that care has to be taken when parameters used for the refinements are selected. In addition to the two medium-strength O—H---O hydrogen bonds, which are found to differ between molecules, the crystal structure exhibits a large array of weak intermolecular hydrogen bonds. These are assessed using a topological analysis of the electron density distribution based on Bader's theory of atoms in molecules. Two discrete groups of hydrogen bonds emerge that could only partly be differentiated using conventional structural crystallography.

Introduction

One of the major advantages of experimental charge density (CD) studies is the unique opportunity it offers to study the influence of such elusive phenomena as crystal field and electron correlation effects on the molecular electron density distribution (EDD).[1] These remain exceedingly computationally expensive to include in theoretical calculations whereas they are implicitly accounted for in the X-ray diffraction intensities. As such, as the electron density is a physical observable, the experimental description of the EDD may appear more rigorous than the theoretical.

Several procedures to obtain quantitative measures for the crystal field effects exist; for instance, can comparative studies of the charge density distribution in different polymorphic forms of a molecule highlight the influence of slightly different environments?[2] However, this approach depends on the successful elimination of systematic errors from independent experiments, which can prove a difficult task. Another method is the study of systems with two crystallographically different molecules coexisting in a crystal structure, i.e., when the crystallographic number Z' is 2 (subsequently called $Z2$ compounds). EDD studies of such $Z2$ compounds are very rare,[3] and in the majority most of these studies the approach has been to treat the different molecular densities as identical. However, it is commonly observed that the two different molecules exhibit quite substantial differences in thermal motion,[4] indicating that the crystal fields experienced by each molecule are dissimilar, and the degree to which this may perturb the molecular densities remains unresolved.

Additionally, the concept of transferability of multipole parameters has in recent years been examined theoretically[5] as well as experimentally.[6] The idea of transferability revolves around the view that the multipole parameters applied in the description of the EDD of a particular chemical entity remain constant over a range of different chemical environments. In principle, this means that crystal field effects are considered negligible, which remains a valid assumption only in certain cases.

In this study, the experimental charge density distribution of the $Z2$ compound 9-ethynyl-9-fluorenol (**1**) is reported and compared to high-level theoretical results. The main emphasis of the current paper is on the potential of the multipole description to model the crystallographically dissimilar molecules in an independent manner. The structure of compound **1**, Figure 1, has previously been determined[7] and it was shown to contain a number of weak C—H---π interactions. These weak hydrogen bonds have in recent years received tremendous interest and have been proposed to play a major role in molecular recognition processes and in the control of crystal growth.[8] Therefore, part of the aim of the present study is to examine this class of weak hydrogen bonds using the charge density approach.

Experimental Section

Single-Crystal X-ray Diffraction Data Collection and Reduction. A suitable single crystal of 9-ethynyl-9-fluorenol was chosen directly from a commercial batch from Sigma-Aldrich. The crystal was mounted on a Bruker SMART 1000 CCD based diffractometer and cooled to 100(2) K using an Oxford Cryostream liquid N_2 device. Six different sets of data were collected using ω-scans of 0.3° to ensure maximum coverage of the reciprocal space to a resolution corresponding to 1.04 Å^{-1}. A total of 77 536 intensities were obtained by integration using the SAINT+ program.[9] An analytical absorption correction was applied to the intensities prior to averaging and outlier rejection with the program SORTAV,[10] which gave 20 334 unique reflections with an average redundancy of 3.8 and an internal agreement of the data of 2.7%. The completeness of the diffraction data was 97.1%.

Refinement Strategies. The structure of **1** was solved from direct methods using the program SHELXS.[11] The positional

* Corresponding author. E-mail: d.hibbs@chem.usyd.edu.au.
[†] University of Sydney.
[‡] Cardiff University.

10.1021/jp036269x CCC: $25.00
Published on Web 11/05/2003

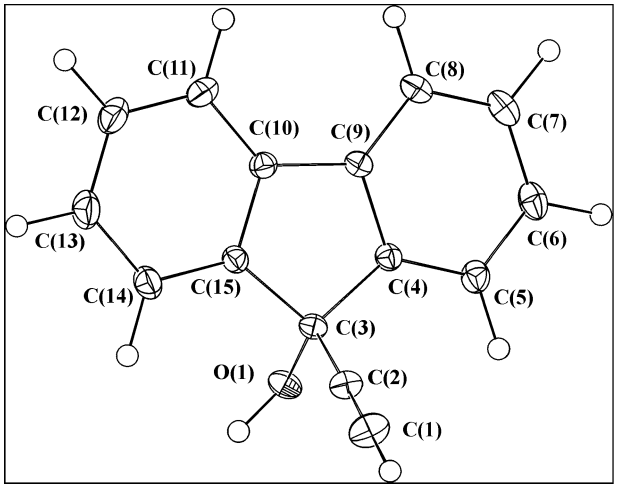

Figure 1. ORTEP drawing of molecule A based on model I, showing 50% probability ellipsoids. Hydrogen atoms (not labeled) are shown as circles.

and thermal parameters and a scale factor were refined to convergence using the IAM model using SHELXL-97[11] ($R(F^2) = 0.047$). This model was imported into the multipole refinement program XD,[12] which is based on the pseudoatomic description of the aspherical electron density suggested by Hansen and Coppens.[13] In this particular framework, the atomic density is described by two spherical contributions, the core density and the valence density, in addition to an aspherical part which outlines the deviation from sphericity of the atomic valence electrons. The core electrons are distinct from the valence electrons in the fact that the latter can be transferred between atoms, thus accounting for the charge transfer within the molecule. Furthermore, the radial distribution of the valence electrons can be refined during the least-squares procedure. The aspherical electron density is described by a set of atom-centered multipole functions similar in appearance to atomic orbital functions, differing only by their normalization. Hartree−Fock wave functions[14] expanded over Slater-type basis functions were used to calculate the density for the two spherical density contributions, whereas simple Slater functions were used to describe the aspherical deformation density.

An initial high-order (HO) refinement (sin $\theta/\lambda > 0.7$ Å^{-1}) was performed to determine the best positional and thermal parameters. The hydrogen atoms were in all refinements positioned so that the X−H bond distances corresponded to tabulated values from neutron diffraction studies.[15] The intention of this study is partly to examine the capabilities of an experimental charge density experiment in determining the small differences between two crystallographically different molecules in the asymmetric unit. For this purpose, four models (models I−IV) were created imposing different levels of constraints on the multipole parameters. Common to all models were three groups of hydrogens, ethynyl H, O−H and C−H, each group assigned one monopole and one bond directed dipole. Noncrystallographic mirror symmetry in the molecular planes was imposed in all models. Furthermore, an electroneutrality constraint prevented any intermolecular charge transfer. In model I, no constraints were imposed on either of the two molecules in **1** (hereafter called A and B). Model II treated the two molecules A and B as identical. In model III, a noncrystallographic mirror-plane was imposed perpendicular to each molecule, such that the following pairs of atoms had identical multipoles: C9−C10, C8−C11, C7−C12, C6−C13, C5−C14, and C4−C15. However, the two molecules remained completely independent.

TABLE 1: Crystallographic Details

chemical formula	$[C_{15}H_{10}O]_2$
chemical formula weight	416.49
crystal system, space group	monoclinic, *C*2/*c*
a (Å)	28.0503(10)
b (Å)	8.5232(3)
c (Å)	22.6161(8)
β (deg)	124.742(1)
V (Å^{-3})	4443.1(4)
Z	8
D_x (Mg m^{-3})	1.245
radiation type, λ (Å)	Mo Kα, 0.7107
no. of reflections for cell refinement	10271
θ range (deg)	2.191−47.282
μ (mm^{-1})	0.08
temperature (K)	100(2)
crystal form, color	rectangular block, colorless
crystal size (mm)	0.25 × 0.28 × 0.48
absorption correction	analytical
T_{min}, T_{max}	0.969, 0.983
no. of measured reflections	77536
no. of independent reflections	20334
no. of observed reflections	15049
criterion for observed reflections	$I > 2\sigma(I)$
R_{int}	0.027
θ_{max}	47.728
completeness (%)	97.1
range of *h*, *k*, *l*	−58 → +57
	0 → 17
	0 → 45
extinction method	Gaussian isotropic
extinction coefficient	0.12(2)
residuals	see text
no. of parameters	674/554/480/447

Finally, model IV was a combination of models II and III. Thus, the two molecules A and B are identical in model IV, as well as the two halves of both A and B. This approach reduces the number of multipole parameters involved to approximately one-fourth of the number employed in model I.

All multipole refinements were started from the same starting structure and carried out to convergence in a stepwise manner. This means that each level of multipole parameters was refined to convergence before the next level was introduced in the refinements. The final models included separate κ-sets for O, C(sp), C(sp^2), C(sp^3), and H. κ'' values, which were refined in separate cycles, were constrained to remain similar for all values of *l*. The final refinements included all structural, thermal, and multipole parameters and resulted in the following agreement factors: $R(F^2) = 0.034/0.035/0.035/0.034$ and $R_w(F^2) = 0.045/0.047/0.047/0.049$ for models I/II/III/IV, respectively.

The Hirshfeld rigid bond test[16] of the initial HO refinement led to an average difference of mean square displacement amplitudes $\langle\Delta_{A-B}\rangle$) for the 36 bonds in **1** (not including bonds to the hydrogens) of 2.9×10^{-4} Å^2, with the largest value being 14×10^{-4} Å^2 for the C(3)−C(4) bond in molecule B. This strongly indicates that the atomic thermal vibrations have already been almost absolutely accounted for using the IAM model, and only small improvements are found upon refinement of the aspherical EDD. Thus, the final $\langle\Delta_{A-B}\rangle$ values are $(2.9-3.2) \times 10^{-4}$ Å^2 for the four refinements. All four models agree that the largest discrepancy remains in molecule B.

Further experimental details are given in Table 1 and in the Supporting Information. The molecule is shown in Figure 1 with thermal probability ellipsoids taken from model I. The residual density map for molecule A from model I is shown in Figure 2.

Molecular Orbital Calculations. Two gas-phase DFT calculations were performed with the GAUSSIAN98 program package[17] at the 6-311++G** level of theory, using the using the three parameter hybrid exchange functional of Becke in

TABLE 2: Comparison of Bond Distances in 1[a]

bond	exp(A)	exp(B)	$10^4\delta$exp	⟨exp⟩	theory	10^4(⟨exp⟩ − theo)
O(1)−C(3)	1.4337(5)	1.4309(5)	28	1.4323	1.4385	−62
C(1)−C(2)	1.2058(5)	1.2062(5)	−4	1.2060	1.2028	32
C(2)−C(3)	1.4731(5)	1.4705(5)	26	1.4718	1.4694	24
C(9)−C(10)	1.4693(5)	1.4689(6)	4	1.4691	1.4717	−26
C(3)−C(4)	1.5265(4)	1.5261(5)	4	1.5263	1.5296	−33
C(3)−C(15)	1.5297(5)	1.5290(5)	7	1.5294	1.5363	−69
	−32	−29		−31	33	
C(4)−C(5)	1.3860(5)	1.3894(5)	−34	1.3877	1.3843	34
C(14)−C(15)	1.3841(5)	1.3873(6)	−32	1.3857	1.3850	7
	19	21		20	−7	
C(4)−C(9)	1.4032(5)	1.3985(5)	47	1.4009	1.4023	−14
C(10)−C(15)	1.4032(4)	1.4078(6)	−46	1.4055	1.4035	20
	0	−93		−46	−12	
C(5)−C(6)	1.4032(6)	1.3994(6)	38	1.4013	1.3982	31
C(13)−C(14)	1.3995(6)	1.4001(9)	−6	1.3998	1.3987	11
	37		−7	15	−5	
C(6)−C(7)	1.3985(6)	1.3986(10)	−1	1.3986	1.3966	20
C(12)−C(13)	1.3981(6)	1.4108(14)	−127	1.4045	1.3960	85
	64	−122		−59	6	
C(7)−C(8)	1.3971(6)	1.3989(10)	−18	1.3980	1.3960	20
C(11)−C(12)	1.4018(6)	1.3975(11)	43	1.3997	1.3963	34
	−47	14		−17	−3	
C(8)−C(9)	1.3926(5)	1.3933(6)	−7	1.3930	1.3932	−2
C(10)−C(11)	1.3962(5)	1.3894(6)	68	1.3928	1.3929	−1
	−36	39		2	3	
av values			−10			
	−55	−177		−116	15	

[a] The experimental values are taken from model I. Integer values in columns 2, 3, 5, and 6 represent the differences between the two bond distances directly above. All values are given in Å, and all differences are multiplied by 10^4.

combination with the gradient corrected exchange-correlation potential of Lee, Yang, and Parr (B3LYP).[18] The first calculation included an optimization of one molecule of 9-ethynyl-9-fluorenol, whereas the other calculation consisted of a single point calculation of the two molecules A and B in the experimental geometry, obtained from model I. A third calculation focused on the central intermolecular O—H---O hydrogen bonding involving four different molecules (tetramer). Thus, a single-point calculation of the four involved molecules was carried out using a lower level of theory (B3LYP/6-31+G(d,p)). The AIMPAC suite of programs[19] was used for the topological analysis of all theoretical wave functions. Calculations were performed on a Silicon Graphics ORIGIN2400 computer [reference: http://www.ac3.com.au/sgi-origin-2400.htm] and on the UKCCF's central Columbus facility.

Results and Discussion

Structural Comparisons. With the result of the Hirshfeld rigid bond test that the smallest value for $\langle\Delta_{A-B}\rangle$ is found in model I, the bond distances listed in Table 2 are from this model. However, the bond lengths from the other models are nearly identical, the largest deviation is in the C(12B)—C(13B) bond, which is 0.003 Å longer in model I. On average, the differences in bond lengths between different models are slightly larger for molecule B than for A. However, these differences are only significant on a 3σ-criterion for the aforementioned C(12B)—C(13B) bond. The listed bond distances are significantly different from the previously published geometry of **1** by Steiner et al.[7]

The title molecule is composed of two similar halves, and Table 2 is therefore formatted such that corresponding bonds from separate halves of the molecule are listed in pairs, with the exception of the four first lines, which represent the only unique bonds in **1**; see also Figure 1. The fourth column in Table 2, outlining the differences between identical bonds in A and B, respectively, shows a large spread of values, compared to the esds on the individual bond distances. However, the differences add up to only 0.0010 Å, which indicates that the sum of bond distance in the two molecules A and B is almost constant. Surprisingly, the differences between the two sides of the molecule in both molecules A and B clearly suggest that the sum of bond distances is not conserved within the molecule. In molecule B this difference is as large as 0.0177 Å, whereas it is less pronounced in molecule A (0.0055 Å). Table 2 also gives the bond distances (column 6) from the theoretically optimized structure of one molecule of 9-ethynyl-9-fluorenol. Column 7 gives the difference of this value and the average experimental bond length in the two independent molecules (column 5). From the differences given in columns 5 and 6 (averages are 0.0116 and 0.0015 Å, respectively) it appears that theory predicts the two halves of 9-ethynyl-9-fluorenol to have more similar bond distances than found experimentally. The only exception to this observation is the two bonds, C(3)—C(4) and C(3)—C(15), which have clearly different lengths in the theoretical calculation. This is probably explained by the different environments near C(4) and C(15) caused by the two different functional groups bonded to C(3) out of the ring plane, i.e., the hydroxyl group and the ethynyl group.

Charge Distribution. The charge density distribution provides another quantitative measure of the crystal field effect, which is perhaps more interesting than the purely structural differences treated in the previous section. In particular, a topological analysis of the charge density using the atoms in molecules (AIM) approach[20] is ideally suited to this purpose. This analysis results in a set of bond critical points (bcps) that can be used to gain detailed information concerning the interatomic bonds. To analyze the electronic differences between the two molecules, selected topological indices evaluated at the bcps for models I−IV, as well as the results for the theoretically optimized (OPT) monomer and the single-point (SP) dimer, are given in Tables 3 and 4.

Several trends can be inferred from Tables 3 and 4. The electron density at the bcp is clearly underestimated in the theoretical calculations, whereas the value of the Laplacian is more negative from theory. This feature has been observed before.[21] This variation is more pronounced in the polar bonds than in the less polar bonds and manifests itself in a different position of the bcp, for instance in the O(1)—C(3) bond, where the experimental bcp is found 0.06 Å closer to O(1) than the theoretical bcp.

As the geometries of the two different molecules A and B are slightly different, as shown in the previous section, it is necessary to consider the effect this may have on the charge distribution. Table 3 therefore also contains the results of the topological analysis of model II, which uses identical multipoles for the two different molecules; hence the topological variations for this model originates chiefly in the geometrical differences. Thus, an estimate of the maximum deviation due to structural discrepancies between A and B are 0.02 e $Å^{-3}$ in ρ_{bcp}, 0.6 e $Å^{-5}$ in $\nabla^2\rho_{bcp}$, and 0.003 Å in the position of the bcp. However, examining the topological analysis for models I and III (which do not constrain the molecules to be identical) reveals significantly larger deviations in equivalent bonds in A and B. The largest deviation in ρ_{bcp} is 0.07 e $Å^{-3}$ whereas the differences in the $\nabla^2\rho_{bcp}$ are as large as 3.0 e $Å^{-5}$. Nevertheless, by far the most noticeable differences between A and B lie in the positions of the bcps. In 10 of the 13 bonds involving sp^2-hybridized carbon atoms in each molecule (the three exceptions being the bonds: C(8)—C(9), C(13)—C(14), and C(14)—C(15)), there is a fundamental difference involving a shift of the bcp from a

TABLE 3: Total Electron Density (ρ_{bcp}) and Laplacian Values ($-\nabla^2\rho_{bcp}$) at the bcps in the Non-H Containing Bonds[a]

	ρ_{bcp} (e Å^{-3})						$-\nabla^2\rho_{bcp}$ (e Å^{-5})					
bond	I	II	III	IV	SP	OPT	I	II	III	IV	Sp	OPT
O(1)−C(3)	1.80	1.82	1.81	1.82	1.72	1.69	6.8	7.1	6.6	7.1	14.1	13.4
	1.86	1.83	1.85	1.83	1.70		8.1	7.4	7.3	7.4	12.6	
C(1)−C(2)	3.03	3.00	3.02	2.99	2.72	2.74	25.6	25.5	25.7	24.8	28.5	28.9
	3.01	3.00	2.98	3.00	2.72		26.3	25.5	25.0	24.9	28.5	
C(2)−C(3)	1.90	1.86	1.89	1.86	1.79	1.80	10.8	10.7	10.8	10.7	16.3	16.6
	1.85	1.87	1.85	1.87	1.80		10.6	10.8	10.6	10.8	16.4	
C(3)−C(4)	1.70	1.71	1.70	1.71	1.69	1.68	8.5	9.0	9.1	9.2	14.2	14.0
	1.74	1.72	1.74	1.72	1.69		9.3	9.1	9.5	9.3	14.1	
C(3)−C(15)	1.71	1.71	1.70	1.70	1.68	1.66	9.1	9.4	8.9	9.1	13.9	13.5
	1.71	1.71	1.72	1.70	1.68		9.5	9.3	9.6	9.1	13.9	
C(4)−C(5)	2.26	2.25	2.27	2.27	2.11	2.11	18.7	18.5	19.4	19.0	21.2	21.3
	2.26	2.25	2.29	2.26	2.10		17.9	18.3	19.1	18.8	20.9	
C(4)−C(9)	2.15	2.18	2.19	2.18	2.08	2.08	16.2	17.2	17.5	16.8	20.5	20.5
	2.22	2.20	2.22	2.19	2.09		18.3	17.4	17.5	17.1	20.6	
C(5)−C(6)	2.17	2.18	2.19	2.18	2.05	2.06	16.6	17.0	17.2	16.8	20.1	20.4
	2.16	2.18	2.17	2.18	2.06		16.9	17.1	17.0	17.0	20.3	
C(6)−C(7)	2.24	2.25	2.23	2.23	2.07	2.07	19.6	19.3	19.0	18.4	20.4	20.6
	2.23	2.25	2.23	2.23	2.08		18.2	19.4	17.8	18.5	20.7	
C(7)−C(8)	2.21	2.20	2.22	2.21	2.07	2.07	18.7	18.3	18.7	17.9	20.4	20.5
	2.16	2.21	2.22	2.21	2.06		15.7	18.3	17.5	17.9	20.3	
C(8)−C(9)	2.19	2.21	2.21	2.21	2.09	2.08	17.1	17.8	17.8	17.7	20.9	20.7
	2.21	2.21	2.23	2.22	2.08		17.7	17.9	18.2	17.7	20.8	
C(9)−C(10)	1.85	1.88	1.88	1.88	1.82	1.81	11.3	12.1	12.2	12.2	16.4	16.2
	1.90	1.88	1.93	1.88	1.82		12.5	12.2	13.6	12.2	16.4	
C(10)−C(11)	2.21	2.22	2.20	2.20	2.07	2.08	17.8	18.0	17.6	17.5	20.5	20.8
	2.26	2.24	2.24	2.22	2.09		18.5	18.3	18.3	17.8	20.9	
C(10)−C(15)	2.21	2.19	2.19	2.18	2.08	2.08	17.6	16.7	17.5	16.9	20.4	20.4
	2.16	2.18	2.20	2.18	2.07		14.8	16.6	17.1	16.8	20.2	
C(11)−C(12)	2.20	2.22	2.20	2.19	2.05	2.07	18.1	18.4	18.3	17.5	20.0	20.5
	2.21	2.24	2.23	2.21	2.08		17.3	19.0	17.5	18.0	20.6	
C(12)−C(13)	2.23	2.24	2.23	2.23	2.07	2.08	18.6	19.1	19.0	18.5	20.4	20.6
	2.26	2.22	2.20	2.21	2.03		18.7	18.6	17.3	18.0	19.6	
C(13)−C(14)	2.23	2.21	2.20	2.18	2.07	2.06	18.4	18.5	17.4	17.0	20.4	20.3
	2.21	2.21	2.17	2.18	2.05		18.3	18.5	17.0	17.0	20.0	
C(14)−C(15)	2.29	2.31	2.27	2.27	2.12	2.11	20.1	20.7	19.5	19.1	21.3	21.1
	2.34	2.30	2.29	2.26	2.10		20.5	20.4	19.1	18.8	20.9	

[a] For each bond, first line gives values from molecule A, and second line vlaues from molecule B. Standard uncertainties have been omitted from the table for clarity. They are closely scattered around 0.02 e Å^{-3} (ρ_{bcp}) and 0.05 e Å^{-5} ($\nabla^2\rho_{bcp}$).

position closer to one atom in molecule A to a position closer to the other atom in molecule B. These differences in the positions of the bcps are not correlated to any differences in other properties of the density or to the bond distances. The reason for this change in the behavior of the EDD could reflect differences in the electronic delocalization within the two molecules. The fact that constrained multipole models that do not allow for such differences to occur are able to describe the EDD equally well (in terms of residual density) underlines the importance of including additional measures to supplement residual factors in the assessment of models. These methods could include topological analysis and mapping of the total charge density and its derivative.

The integration of atomic charges within the atomic basins as defined by the zero-flux surfaces of the density may provide additional insight into the consequences of the above-mentioned charge redistribution. Table 5 lists this property for the four different refinements calculated from the multipole models using the program TOPXD.[22]

The atomic charges for all refinements add up to neutral molecules within 0.04 e$^-$. The most conspicuous result in Table 5 is the consistently highly charged hydrogen atom H(1O), which has lost around 70% of its only electron. It is also noteworthy that there is a significant spread in the atomic charges of the other hydrogen atoms. Models II and III have hydrogen atomic charges +0.15 higher than models I and IV for both the ethynyl hydrogen and the eight aromatic carbon-bonded hydrogens. This corresponds well with an average excess negative charges of −0.09 e$^-$ on the twelve aromatic carbon atoms (C(4) to C(15)) in models II and III. It is interesting to compare the two molecules (A and B) in refinement I to estimate the influence of the altered density distribution. Considering first C(9) and C(10), we observe that they carry virtually identical charges in both molecules in model I. This occurs despite the highly significant difference between A and B in the position of their shared bcp and is explained by a simultaneous change in the position of the bcps in the other bonds in which C(9) and C(10) take part to oppose the effect. Second, if we consider C(5) and C(8) in model I, we find that they possess atomic charges differing more than 0.1 e$^-$. In A, C(5) is positive and C(8) is negative whereas exactly the opposite is the situation in B. The same trend can be found for C(11) and C(14), although the values here may not be significant. This testifies of a variation in delocalization within the aromatic system that disappears upon the implementation of chemical constraints in the refinement procedure.

In summary, we observe that the variation in crystal field may be responsible for a significant change in the molecular charge distribution. The difference in the molecular EDDs can be represented by the electrostatic potential calculated separately for molecule A (Figure 3a) and B (Figure 3b) using model I. In the close proximity of the molecule, the ESPs look identical. However, further away from the molecule there appears to be some asymmetry in molecule B, which is not present for molecule A.

Hydrogen Bonding and the Charge Density. In the previous section differences between the EDD in the different models were established. However, these differences do not pertain to the intermolecular interaction in any significant extent and the remainder of this paper uses results from model I. Compound **1** offers the opportunity to study HBs covering a large range of bond strengths. There are medium-strength O—H---O HBs as

TABLE 4: Distance from First (1) and Second Atom (2) to Their Shared Bond Critical Point[a]

	d_{1-bcp} (Å)					d_{2-bcp} (Å)						
bond	I	II	III	SP	OPT	I	II	III	III	IV	SP	OPT
O(1)−C(3)	0.830	0.826	0.827	0.825	0.900	0.907	0.604	0.609	0.607	0.609	0.534	0.532
	0.822	0.825	0.821	0.824	0.913		0.609	0.606	0.610	0.606	0.518	
C(1)−C(2)	0.635	0.643	0.640	0.644	0.590	0.589	0.570	0.562	0.565	0.562	0.616	0.613
	0.643	0.643	0.648	0.644	0.591		0.562	0.562	0.558	0.562	0.615	
C(2)−C(3)	0.753	0.753	0.757	0.752	0.775	0.771	0.720	0.720	0.716	0.721	0.698	0.698
	0.747	0.751	0.752	0.751	0.770		0.723	0.719	0.719	0.719	0.701	
C(3)−C(4)	0.768	0.762	0.759	0.764	0.775	0.781	0.759	0.765	0.767	0.763	0.752	0.749
	0.762	0.762	0.762	0.764	0.781		0.764	0.764	0.764	0.762	0.745	
C(3)−C(15)	0.766	0.768	0.763	0.765	0.772	0.778	0.765	0.762	0.767	0.765	0.758	0.759
	0.774	0.768	0.761	0.766	0.778		0.755	0.762	0.769	0.765	0.752	
C(4)−C(5)	0.706	0.691	0.706	0.698	0.700	0.701	0.680	0.695	0.680	0.688	0.685	0.683
	0.664	0.692	0.700	0.698	0.703		0.725	0.696	0.688	0.689	0.685	
C(4)−C(9)	0.685	0.699	0.696	0.700	0.702	0.702	0.718	0.704	0.707	0.704	0.701	0.700
	0.708	0.697	0.702	0.698	0.702		0.690	0.702	0.699	0.702	0.698	
C(5)−C(6)	0.679	0.689	0.699	0.704	0.702	0.701	0.724	0.714	0.704	0.698	0.700	0.697
	0.712	0.687	0.711	0.703	0.702		0.687	0.713	0.689	0.697	0.697	
C(6)−C(7)	0.648	0.667	0.671	0.684	0.697	0.697	0.750	0.732	0.727	0.716	0.701	0.700
	0.726	0.667	0.711	0.683	0.695		0.675	0.731	0.689	0.715	0.700	
C(7)−C(8)	0.672	0.706	0.698	0.701	0.698	0.697	0.725	0.691	0.699	0.697	0.700	0.700
	0.780	0.706	0.706	0.701	0.697		0.618	0.691	0.692	0.697	0.701	
C(8)−C(9)	0.696	0.697	0.698	0.699	0.688	0.688	0.696	0.696	0.695	0.694	0.704	0.706
	0.701	0.697	0.690	0.698	0.686		0.693	0.696	0.703	0.694	0.707	
C(9)−C(10)	0.730	0.753	0.735	0.735	0.735	0.735	0.741	0.717	0.735	0.735	0.736	0.737
	0.800	0.753	0.735	0.735	0.735		0.670	0.717	0.735	0.735	0.735	
C(10)−C(11)	0.682	0.689	0.696	0.696	0.706	0.705	0.714	0.707	0.699	0.700	0.690	0.688
	0.696	0.687	0.702	0.694	0.704		0.694	0.705	0.689	0.698	0.687	
C(10)−C(15)	0.698	0.704	0.707	0.704	0.701	0.700	0.705	0.701	0.696	0.700	0.702	0.704
	0.719	0.705	0.701	0.705	0.701		0.690	0.702	0.705	0.700	0.705	
C(11)−C(12)	0.680	0.707	0.701	0.699	0.702	0.699	0.721	0.695	0.700	0.703	0.700	0.696
	0.780	0.704	0.692	0.696	0.698		0.619	0.692	0.706	0.700	0.696	
C(12)−C(13)	0.693	0.696	0.726	0.715	0.701	0.698	0.704	0.702	0.671	0.683	0.697	0.697
	0.716	0.700	0.692	0.718	0.704		0.697	0.705	0.714	0.686	0.704	
C(13)−C(14)	0.669	0.679	0.702	0.697	0.698	0.696	0.730	0.720	0.697	0.703	0.699	0.703
	0.693	0.679	0.688	0.697	0.697		0.706	0.720	0.710	0.703	0.704	
C(14)−C(15)	0.692	0.682	0.679	0.688	0.685	0.686	0.692	0.702	0.705	0.697	0.699	0.699
	0.670	0.684	0.688	0.690	0.686		0.717	0.703	0.700	0.699	0.702	

[a] For each bond, the first line gives values from molecule A, and second line values from molecule B.

TABLE 5: Atomic Charges

atom	$q(\Omega)$,IA	$q(\Omega)$,IB	$q(\Omega)$,II	$q(\Omega)$,IIIA	$q(\Omega)$,IIIB	$q(\Omega)$,IV
O(1)	−1.53	−1.41	−1.45	−1.50	−1.41	−1.45
C(1)	−0.29	−0.30	−0.41	−0.38	−0.43	−0.30
C(2)	−0.12	−0.07	−0.13	−0.17	−0.07	−0.09
C(3)	+0.35	+0.40	+0.39	+0.38	+0.41	+0.39
C(4)	−0.08	−0.07	−0.08	−0.12	−0.14	−0.06
C(5)	+0.03	−0.11	−0.17	−0.11	−0.20	−0.06
C(6)	+0.04	−0.05	−0.15	−0.14	−0.17	−0.03
C(7)	+0.07	+0.04	−0.11	−0.12	−0.07	−0.01
C(8)	−0.12	+0.01	−0.22	−0.23	−0.18	−0.10
C(9)	−0.02	−0.03	−0.03	−0.04	−0.04	−0.01
C(10)	+0.03	+0.01	+0.01	−0.04	−0.05	−0.00
C(11)	−0.08	−0.16	−0.25	−0.22	−0.17	−0.10
C(12)	+0.01	+0.05	−0.14	−0.12	−0.06	−0.01
C(13)	−0.01	+0.02	−0.17	−0.14	−0.16	−0.04
C(14)	−0.07	−0.04	−0.20	−0.12	−0.20	−0.06
C(15)	−0.03	−0.12	−0.06	−0.10	−0.16	−0.06
H(1O)	+0.75	+0.64	+0.67	+0.72	+0.61	+0.70
H(1)	+0.31	+0.28	+0.44	+0.43	+0.46	+0.29
H(5)	+0.10	+0.11	+0.26	+0.25	+0.26	+0.13
H(6)	+0.10	+0.12	+0.26	+0.26	+0.25	+0.12
H(7)	+0.07	+0.09	+0.24	+0.24	+0.25	+0.11
H(8)	+0.10	+0.14	+0.26	+0.25	+0.26	+0.13
H(11)	+0.10	+0.11	+0.26	+0.26	+0.27	+0.13
H(12)	+0.09	+0.13	+0.26	+0.24	+0.25	+0.11
H(13)	+0.10	+0.11	+0.26	+0.26	+0.26	+0.12
H(14)	+0.09	+0.11	+0.25	+0.25	+0.26	+0.12

well as significantly weaker C—H---O and C—H---π HBs. The previous study of **1** was mainly aimed at the investigation of the alkyne C≡C—H---π interaction in a structural sense;[7] however, the present study was undertaken to carry out a more elaborate description of the entire range of HBs available in compound **1**. The geometries and the results of the topological analyses of the X—H---O HBs are given in Table 6.

Using a semiempirical relation between energy densities and topological indices, proposed by Abramov[23] to be valid in the interatomic regions for mainly electrostatic interactions such as hydrogen bonds and metal−ligand interactions, we have also estimated the potential and total energy density in Table 6. The relative sizes of V for the two HBs support the view from the geometry (shorter H---O distance) and topology (higher density at the bcp), that the first HB is the stronger of the two O—H---O HBs. Additionally, Espinosa et al.[24] established a correlation between the theoretically calculated hydrogen bond energies and their corresponding potential energy densities and we have applied this here to estimate the hydrogen bond energies, *E*, in Table 6. This shows again the higher strength of the first HB. Furthermore, it is obvious that the O—H---O HBs are an order of magnitude stronger than the C—H---O HB.

The hydrogen atoms in the O—H---O HBs are directed toward the electronic lone pairs on the acceptor oxygen atom, as is illustrated with the Laplacian plot shown in Figure 4. Hibbs et

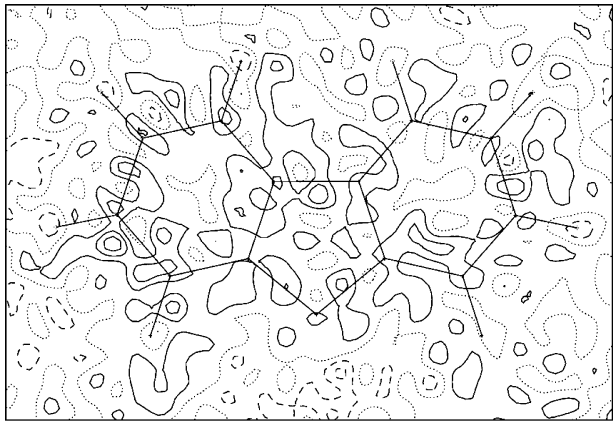

Figure 2. Residual density map of molecule A in model I. Positive and negative contours are shown with solid and dashed lines, respectively, at a contour interval of ±0.10 e Å^{-3}. Labels as in Figure 1.

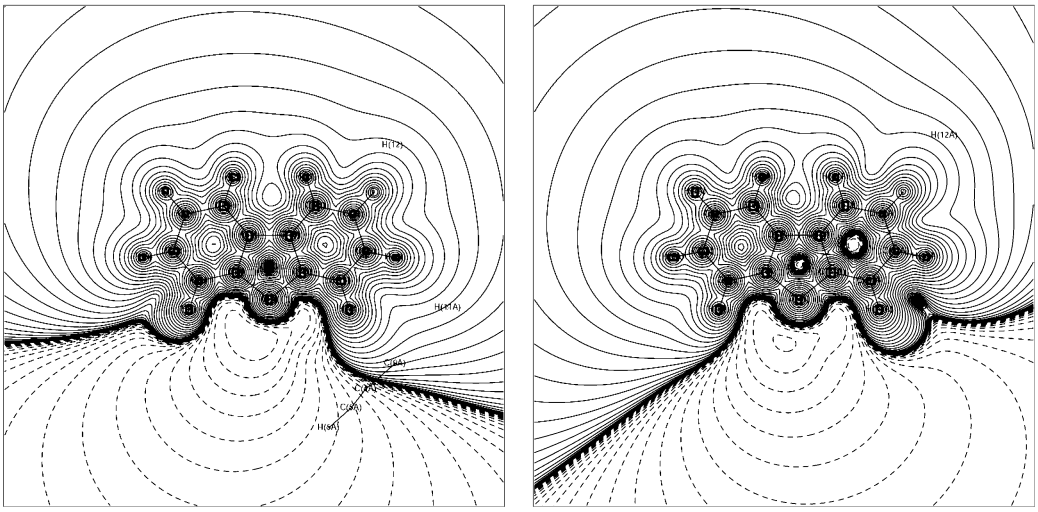

Figure 3. Electrostatic potential in molecule A (left) and B (right) from model I. Contours are shown at $\pm 10^{-6} \times 1.5^{n}$ e Å^{-1}, with $n = 0, 1, 2, ..., 48, 49, 50$.

TABLE 6: Hydrogen Bonds Involving Oxygen[a]

bond	D(H---O)	∠(X−H---O)	ρ_{bcp}	$\nabla^2\rho_{bcp}$	∠H−bcp−O	d(H−bcp)	V	H	E
O(1A)−H(1OA)---O(1B)[i]	1.81	162.6	0.21 (0.22)	3.74 (2.45)	175.8	0.623	−0.21 (−0.17)	0.03	9.7
O(1B)−H(1OB)---O(1A)	1.87	154.2	0.14 (0.20)	3.25 (2.08)	160.3	0.652	−0.13 (−0.15)	0.05	6.0
C(12B)−H(12B)---O(1B)	2.47	156.4	0.03	0.75	160.9	0.973	−0.01	0.01	0.5

[a] Distances given in Å, angles in degrees, ρ_{bcp} in e Å^{-3}, $\nabla^2\rho_{bcp}$ in e Å^{-5}, potential (V) and total (H) energy densities in hartree bohr^{-3}, bond energy (E) in kcal mol^{-1}. Topological results from the tetramer calculation are given in parentheses.

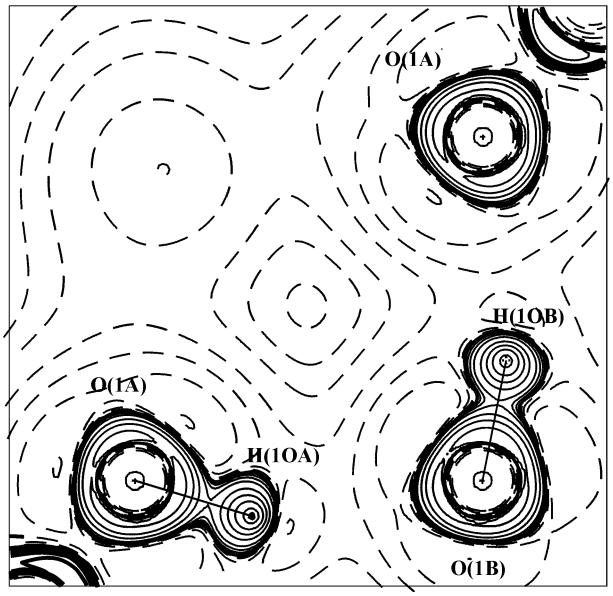

Figure 4. Experimental negative Laplacian map showing the two intermolecular O−H−O HBs in **1**. Solid lines show positive contours; negative contours are shown with dashed lines. The contour interval is ± 0.001 and 2, 4, 8×10^{n}, ($n = -3, -2, -1, 0, 1, 2$) in units of e Å^{-5}.

al.[25] have previously experimentally studied the concept of directionality between hydrogen bond and lone pairs. As an extension to this study the lone pair positions of the O(1A) and O(1B) were located. The C═O---H angles are 135.7 and 132.5° for the two HBs, respectively. However, in agreement with the findings in ref 25, the lone pair positions are not on the line of interaction between the acceptor oxygen and the hydrogen, as the C═O---LP angles are 115.7 and 123.0°.

The results for the C−H---π HBs are given in Table 7. One conspicuous observation in this table is the existence of bcps in a significant number of C−H---π interactions. The positions of the bcps in the crystal structure are shown in Figure 5.

Table 7 suggests the existence of two different types of C−H---π interactions. The seven HBs can be grouped in two classes, the first four separately from the three last HBs. The characteristics of the first group are a distance from H to the acceptor atom of 2.6 Å and a Laplacian close to 0.6 e Å^{-5}. The second group consists of longer interactions, 2.8−2.9 Å, and a Laplacian smaller than 0.4 e Å^{-5}. However, considering the value of the density at the critical point, ρ_{bcp}, the differences are within standard errors. Thus, ρ_{bcp} appears to be too crude a measure to distinguish between types of hydrogen bonds. It is worth noticing that the C≡C−H group acts as both a donor and an acceptor. The trace of the bond paths in these hydrogen bonds shows considerable differences, with the bcp displaced away from the straight line between the two atoms; instead, it is displaced toward the closest neighboring atom in the donor molecule. The considerable curvature of the bond path suggests that the acceptor atom is not just one atom, but the π-density in the aromatic ring. In fact, this situation occurs for all HBs but the ones with the ethynyl group in the role of the acceptor group, that is, interactions 1−3 and 5−6 in Table 7. For graphical representations of bond paths, see the Supporting Information.

Intermolecular Interaction Energies. Recently, the experimental charge density approach (ECDA) has been shown to lead to reasonable results for the intermolecular interaction energies, E_{int}.[26] The ECDA approach is based on an evaluation of the electrostatic intermolecular interaction energy,[27] which in principle includes the crystal effects such as polarization, intramolecular charge transfer and electron correlation. For **1**, the calculation of E_{int} gives −63.5(90) kJ mol^{-1}. This lattice energy is constituted of a significant amount of dispersion energy (−298 kJ mol^{-1}). However, the exchange-repulsion energy (361

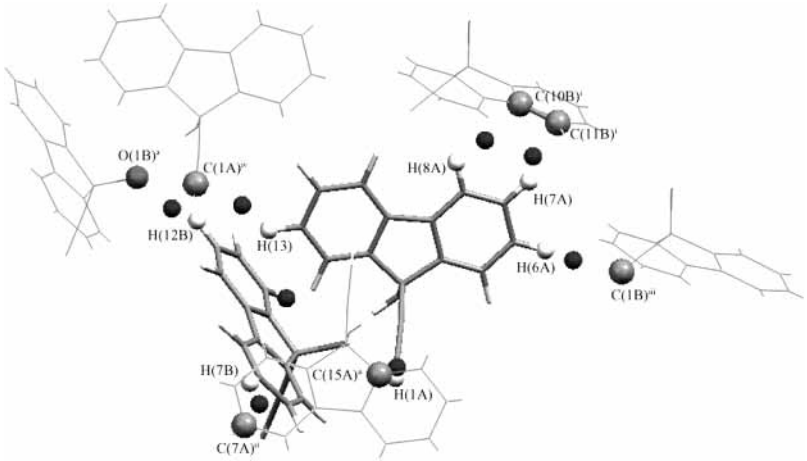

Figure 5. Packing plot of **1**. The two molecules of the asymmetric unit are distinguished from the symmetry-related molecules by their style (wireframe-style used for symmetry-related molecules.) The smaller, darker spheres represent the bcps, given in Table 7, whereas the atoms involved in bonding are highlighted using white (hydrogens) and light gray (C and O) spheres.

TABLE 7: Geometry and Topological Analysis of the Weak C−H−π HBs in 1[a]

bond	type	d(H−A)	ρ_{bcp}	$\nabla^2\rho_{bcp}$
C(7A)−H(7A)−C(11B)[b]	C_{ar}−H---π	2.657	0.04(1)	0.62(1)
C(14A)−H(14A)−C(9B)	C_{ar}−H---π	2.532	0.04(1)	0.62(1)
C(7B)−H(7B)−C(7A)[c]	C_{ar}−H---π	2.593	0.04(1)	0.58(1)
C(6A)−H(6A)−C(1B)[d]	C_{ar}−H---π	2.589	0.03(1)	0.61(1)
C(8A)−H(8A)−C(10B)[b]	C_{ar}−H---π	2.919	0.03(1)	0.38(1)
C(1A)−H(1A)−C(15A)[c]	C≡C−H---π	2.936	0.03(1)	0.35(1)
C(13A)−H(13A)−C(1A)[e]	C_{ar}−H---π	2.810	0.02(1)	0.34(1)

[a] Units used for distances are Å, e Å^{-3} for ρ_{bcp}, and e Å^{-5} for $\nabla^2\rho_{bcp}$. [b] x, 1 − y, 0.5 + z. [c] −x, 1 − y, −z. [c] x, 2 − y, 0.5 + z. [d] x, −1 + y, z.

kJ mol^{-1}) is significantly larger than the electrostatic contributions (−124 kJ mol^{-1}), mainly due to repulsive monopole−quadrupole energy of 163 kJ mol^{-1}.

Conclusion

The experimental and theoretical charge density study of **1** has highlighted the differences that may be anticipated between identical molecules in slightly altered crystal fields. The differences are shown to be of rather fundamental nature, giving information that may be lost if too many approximations are imposed in the process of selecting parameters for an electron density study.

The study of the weak hydrogen bonds in the title compound has led to a more comprehensive understanding of the hydrogen bonds in **1** compared to more straightforward structural and spectroscopic methods, which once again illustrates the applicability of this kind of study. In particular, the finding that the weak C−H−π interactions group roughly in two categories and the pronounced curvature of the bond paths represent results that are a direct consequence of the experimental charge density method. The stronger O−H---O hydrogen bonds are, in accordance with other experimental findings, found to exhibit less directionality than theoretically predicted.

Acknowledgment. We thank the Australian Research Council for funding this work and the Australian Centre for Advanced Computing and Communications (ac3) for a generous allocation of computer resources. D.E.H. also thanks the Royal Society of Chemistry for a Journals Grant. J.O. thanks the Danish Research Council for financial support.

Supporting Information Available: Crystallographic cif file for **1**. Additional model contour maps and bond path material collected in a pdf file. This material is available free of charge via the Internet at http://pubs.acs.org.

Note Added after ASAP Posting. This paper was published ASAP 11/5/2003 without James A. Platts listed as an author and with an incorrect affiliation for Mark P. Waller. The corrected version was posted 11/18/2003.

References and Notes

(1) Koritsanszky, T.; Coppens, P. *Chem. Rev.* **2001**, *101*, 1583−1627.

(2) Gopalan, R. S.; Kulkarni, G. U.; Rao, C. N. R. *ChemPhysChem* **2000**, *1*, 127−135. Kulkarni, G. U.; Gopalan, R. S.; Rao, C. N. R. *J. Mol. Struct. (THEOCHEM)* **2000**, *500*, 339−362. Ferenczy, G. G.; Parkanyi, L.; Angyan, J. G.; Kalman, A.; Hegedus, B. *J. Mol. Struct. (THEOCHEM)* **2000**, *503*, 73−79.

(3) Pichon-Pesme, V.; Lecomte, C. *Acta Crystallogr. Sect. B* **1998**, *54*, 485−493. Hambley, T. W.; Hibbs, D. E.; Turner, P.; Howard, S. T.; Hursthouse, M. B. *J. Chem. Soc., Perkin Trans. 2* **2002**, *2*, 235−239. Overgaard, J.; Schiøtt, B.; Larsen, F. K.; Iversen, B. B. *Chem. Eur. J.* **2001**, *7*, 3756−3767.

(4) For examples, see: Gunes B.; Ozbey S.; Tezcan H. *Anal. Sci.* **2003**, *19*, 1091−1092. Skakle, J. M. S.; Wardell, J. L.; Low, J. N.; Glidewell, C. *Acta Crystallogr. Sect. C* **2001**, *57*, 742−746.

(5) Bader, R. F. W.; Becker, P. *Chem. Phys. Lett.* **1988**, *148*, 452−458. Bader, R. F. W.; Larouche, A.; Gatti, C.; Carroll, M. T.; MacDougall, P. J.; Wiberg, K. B. *J. Chem. Phys.* **1987**, *87*, 1142−1152. Whitehead, C. E.; Breneman, C. M.; Sukumar, N.; Ryan, M. D. *J. Comput. Chem.* **2003**, *24*, 512−529. Bader, R. F. W.; Bayles, D. *J. Phys. Chem. A* **2000**, *104*, 5579−5589. Kedzierski, P.; Sokalski, W. A. *J. Comput. Chem.* **2001**, *22*, 1082−1097.

(6) Pichon-Pesme, V.; Lecomte, C.; Lachekar, H. *J. Phys. Chem.* **1995**, *99*, 6242. Koritsanszky, T.; Volkov, A.; Coppens, P. *Acta Crystallogr. Sect. A* **2002**, *58*, 464−472.

(7) Steiner, T.; Starikov, E. B.; Amado, A. M.; Teixeira-Dias, J. J. *J. Chem. Soc., Perkin Trans. 2* **1995**, 1321−1326.

(8) Desiraju, G. R.; Steiner, T. *The Weak Hydrogen Bond*; Oxford University Press: Oxford, 1999. Langley, P. J.; Hulliger, J.; Thaimattam, R.; Desiraju, G. R. *New J. Chem.* **1998**, *22*, 1307−1309. Keegstra, E. M. D.; van der Mieden, V.; Zwikker, J. W.; Jenneskens, L. W.; Schouten, A.; Kooijman, H.; Veldman, N.; Spek, A. L. *Chem. Mater.* **1996**, *8*, 1092−1105. Hanessian, S.; Gomtsyan, A.; Simard, M.; Roelens, S. *J. Am. Chem. Soc.* **1994**, *116*, 4495−4496. Steiner, T. *Angew. Chem., Int. Ed.* **2002**, *41*, 48−76.

(9) *SAINT: Area-Detector Integration Software*; Siemens Industrial Automation, Inc.: Madison, WI, 1995.

(10) Blessing, R. H. SORTAV. *Cryst. Rev.* **1987**, *1*, 3−58.

(11) Sheldrick, G. M. SHELX97 − Programs for Crystal Structure Analysis (Release 97-2). Institüt für Anorganische Chemie der Universität, Tammanstrasse 4, D-3400 Göttingen, Germany, 1998.

(12) Koritsanszky, T.; Howard, S. T.; Macchi, P.; Gatti, C.; Farrugia, L. J.; Mallinson, P. R.; Volkov, A.; Su, Z.; Richter, T.; Hansen, N. K. *XD. A Computer Program Package for Multipole Refinement and Analysis of*

Charge Densities from X-ray Diffraction Data; Free University of Berlin: Germany, 2003.

(13) Hansen, N. K.; Coppens, P. *Acta Crystallogr. Sect. A* **1979**, *39*, 909−921.

(14) Clementi, E.; Roetti, X. *J. Chem. Phys.* **1963**, *41*, 2686.

(15) Allen, F. H.; Kennard, O.; Watson, D. G.; Brammer, L.; Orpen, A. G.; Taylor, R. *J. Chem. Soc., Perkin Trans. 2* **1987**, S1−S9.

(16) Hirshfeld, F. L. *Acta Crystallogr.* **1976**, *A32*, 239−244.

(17) Frisch, M. J.; Trucks, G. W.; Schlegel, H. B.; Scuseria, G. E.; Robb, M. A.; Cheeseman, J. R.; Zakrzewski, V. G.; Montgomery, J. A., Jr.; Stratmann, R. E.; Burant, J. C.; Dapprich, S.; Millam, J. M.; Daniels, A. D.; Kudin, K. N.; Strain, M. C.; Farkas, O.; Tomasi, J.; Barone, V.; Cossi, M.; Cammi, R.; Mennucci, B.; Pomelli, C.; Adamo, C.; Clifford, S.; Ochterski, J.; Petersson, G. A.; Ayala, P. Y.; Cui, Q.; Morokuma, K.; Malick, D. K.; Rabuck, A. D.; Raghavachari, K.; Foresman, J. B.; Cioslowski, J.; Ortiz, J. V.; Stefanov, B. B.; Liu, G.; Liashenko, A.; Piskorz, P.; Komaromi, I.; Gomperts, R.; Martin, R. L.; Fox, D. J.; Keith, T.; Al-Laham, M. A.; Peng, C. Y.; Nanayakkara, A.; Gonzalez, C.; Challacombe, M.; Gill, P. M. W.; Johnson, B. G.; Chen, W.; Wong, M. W.; Andres, J. L.; Head-Gordon, M.; Replogle, E. S.; Pople, J. A. *Gaussian 98*, revision A.7; Gaussian Inc.: Pittsburgh, PA, 1999.

(18) Becke, A. D.; *J. Chem. Phys.* **1993**, *98*, 5648−5652. Lee, C.; Yang. W.; Parr, R. G. *Phys. Rev. B* **1988**, *38*, 785−789. Stevens, P. J.; Devlin, F. J.; Chabalowski, C. F.; Frisch, M. J. *J. Phys. Chem.* **1994**, *98*, 11623−11627. Adamo, C.; Barone, V. *Chem. Phys. Lett.* **1997**, *274*, 242−250.

(19) Biegler-König, F. W.; Bader, R. F. W.; Ting-Hua, T. *J. Comput. Chem.* **1982**, *3*, 317.

(20) Bader, R. F. W. *Atoms in Molecules − A Quantum Theory*; Clarendon Press: Oxford, U.K., 1990.

(21) Flaig, R.; Koritsanszky, T.; Zobel, D.; Luger, P. *J. Am. Chem. Soc.* **1998**, *120*, 2227−2238. Koritsanszky, T.; Buschmann, J.; Lentz, D.; Luger, P.; Perpetuo, G.; Rottger, M. *Chem. Eur. J.* **1999**, *5*, 3413−3420.

(22) Volkov, A.; Gatti, C.; Abramov, Yu. A.; Coppens, P. *Acta Crystallogr. Sect. A* **2000**, *56*, 252.

(23) Abramov, Yu. A. *Acta Crystallogr. Sect. A* **1997**, *53*, 264−272.

(24) Espinosa, E.; Lecomte, C.; Molins, E. *Chem. Phys. Lett.* **1998**, *285*, 170−173.

(25) Hambley, T. W.; Hibbs, D. E.; Turner, P.; Howard, S. T.; Hursthouse, M. B. *J. Chem. Soc., Perkin Trans. 2* **2002**, *2*, 235−239. Hibbs, D. E.; Hanrahan, J. R.; Hursthouse, M. B.; Knight, D. W.; Overgaard, J.; Turner, P.; Piltz, R. O.; Waller, M. P. *Org. Biomol. Chem.* **2003**, *1*, 1034−1040.

(26) Abramov, Yu. A.; Volkov, A.; Wu, G.; Coppens, P. *Acta Crystallogr. Sect. A* **2000**, *56*, 585−591.

(27) Coppens, P. *X-ray Charge Densities and Chemical Bonding*; Oxford Science Publications: Oxford, U.K., 1997.